Spectroscopic, Voltammetric, and Electrochemical Scanning Tunneling Microscopic Study of Underpotentially Deposited Cu Corrosion and Passivation with Self-Assembled Organomercaptan Monolayers

Francis P. Zamborini, Joseph K. Campbell, and Richard M. Crooks*

Department of Chemistry, Texas A&M University, P.O. Box 300012, College Station, Texas 77842-3012

Received August 11, 1997. In Final Form: November 24, 1997

FTIR−external reflectance spectroscopy (FTIR-ERS), X-ray photoelectron spectroscopy (XPS), electrochemistry, and electrochemical scanning tunneling microscopy (ECSTM) were used to study the effect of aromatic and linear-chain thiol adsorbates on the oxidation of underpotentially deposited Cu on Au (Au/Cu-UPD) in $HClO_4$-containing electrolyte solutions. The morphology of the corroding Cu layer and its stripping potential are influenced by the presence of the organomercaptan self-assembled monolayers (SAMs). For *n*-alkanethiol SAMs, the Cu-UPD stripping potential shifts positive as the SAM thickness increases. Aromatic SAMs were found to passivate the Cu−UPD surface more effectively than linear-chain SAMs of equal thickness. Furthermore, a methyl-terminated aromatic SAM shifts the potential for Cu−UPD oxidation more positive than a hydroxy-terminated aromatic SAM. For longer chain *n*-alkanethiol SAMs, the presence of the Cu−UPD layer markedly improves the stability of the SAM compared to when it is adsorbed directly on the Au surface. These findings raise the possibility for new strategies to prevent corrosion using very thin, easily prepared composite films.

Introduction

We report a spectroscopic, voltammetric, and electrochemical scanning tunneling microscopic (ECSTM) study of the corrosion passivation properties of aromatic and linear-chain organomercaptan self-assembled monolayers (SAMs) on underpotentially deposited Cu (Cu−UPD) in aqueous $HClO_4$. This study follows our earlier examination of corrosion passivation of Au by SAMs in the presence of CN^- and Br^-.[1,2] Although Au/Cu−UPD has different properties than bulk Cu, we have chosen to study the UPD system for two reasons. First, the Au/Cu−UPD system is especially good for studying the very early stages of Cu corrosion, since it is possible to observe the time-dependent dissolution of exactly one atomic layer of Cu. This is particularly useful for ECSTM studies, since without a stop-etch layer (Au in the present case) it is difficult to know the total number of layers etched. Second, recent studies by Jennings and Laibinis show that SAMs form on UPD layers of Ag and Cu and that Ag UPD layers stabilize SAM adlayers.[3,4] Therefore, this approach permits us to learn how different types of SAMs affect the initial stages of Cu corrosion.

Cu is a commercially important metal because of its high thermal and electronic conductivity, strength, and decorative appearance. Cu and its alloys are widely used in the electronics industry, in heating and cooling systems, for domestic water pipes, and in architectural metal work.[5] Cu is a fairly noble metal but reacts quickly in air to form a stable oxide. Corrosion of Cu can lead to pitting, staining, or tarnishing of the surface. Accordingly, there is a great deal of interest in understanding the initial stages of Cu corrosion and determining new methods to passivate Cu surfaces.

The Au/Cu−UPD system has been studied previously in aqueous $HClO_4$[6,7] and H_2SO_4[7−13] electrolyte solutions by electrochemistry,[8,12] ECSTM,[6,9−11,13] electrochemical atomic force microscopy (ECAFM),[7] and other analytical methods.[12] Most of the studies involving in-situ scanning probe techniques have focused on determining the potential-dependent, atomically resolved Cu adlayer structure. However, Green and Hanson[10] have studied deposition and stripping of Cu UPD on Au(111) at the nanometer scale in H_2SO_4 electrolytes containing Cu^{2+}.

There is a vast literature dealing with corrosion of Cu and its alloys under various conditions as studied by classical electrochemical methods.[14−19] The few studies that employed scanning probe techniques (AFM, STM)

* To whom correspondence should be addressed. E-mail: crooks@chemvx.tamu.edu. Fax: 409-845-1399. Telephone: 409-845-5629.

(1) Zamborini, F. P.; Crooks, R. M. *Langmuir*, submitted for publication.
(2) Zamborini, F. P.; Crooks, R. M. *Langmuir* **1997**, *13*, 122−126.
(3) Jennings, G. K.; Laibinis, P. E. *J. Am. Chem. Soc.* **1997**, *119*, 5208−5214.
(4) Jennings, G. K.; Laibinis, P. E. *Langmuir* **1996**, *12*, 6173−6175.
(5) Walker, R. *Anti-corrosion* **1970**, *17*, 9−15.
(6) Hotlos, J.; Magnussen, O. M.; Behm, R. J. *Surf. Sci.* **1995**, *335*, 129−144.
(7) Manne, S.; Hansma, P. K.; Massie, J.; Elings, V. B.; Gewirth, A. A. *Science* **1991**, *251*, 183−186.
(8) Omar, I. H.; Pauling, H. J.; Jüttner, K. *J. Electrochem. Soc.* **1993**, *140*, 2187−2192.
(9) Hachiya, T.; Honbo, H.; Itaya, K. *J. Electroanal. Chem.* **1991**, *315*, 275−291.
(10) Green, M. P.; Hanson, K. J. *J. Vac. Sci. Technol. A* **1992**, *10*, 3012−3018.
(11) Magnussen, O. M.; Hotlos, J.; Nichols, R. J.; Kolb, D. M.; Behm, R. J. *Phys. Rev. Lett.* **1990**, *64*, 2929−2932.
(12) Zhang, J.; Sung, Y.-E.; Rikvold, P. A.; Wieckowski, A. *J. Chem. Phys.* **1996**, *104*, 5699−5712.
(13) Möller, F. A.; Magnussen, O. M.; Behm, R. J. *Phys. Rev. B* **1995**, *51*, 2484−2490.
(14) Barcia, O. E.; Mattos, O. R.; Pebere, N.; Tribollet, B. *J. Electrochem. Soc.* **1993**, *140*, 2825−2832.
(15) Hack, H. P.; Pickering, H. W. *J. Electrochem. Soc.* **1991**, *138*, 690−695.
(16) Georgiadou, M.; Alkire, R. *J. Electrochem. Soc.* **1993**, *140*, 1340−1347.
(17) Brossard, L. *J. Electrochem. Soc.* **1983**, *130*, 403−405.
(18) Braun, M.; Nobe, K. *J. Electrochem. Soc.* **1979**, *126*, 1666−1671.

S0743-7463(97)00905-0 CCC: $15.00 © 1998 American Chemical Society
Published on Web 02/03/1998

included corrosion of Cu and its alloys in ClO_4^-,[20] Cl^-,[21-24] and SO_4^{2-}.[25-28] Some of these are particularly relevant to the present study. For example, Suggs and Bard[22] used in-situ STM to study the corrosion of Cu(111) in aqueous Cl^- solution. At corrosive potentials, they found that etching occurs preferentially at step edges along the {211} direction. The use of organomercaptan SAMs as barriers toward Cu corrosion has also been reported previously. Whitesides et al. were the first to report on the properties of *n*-alkanethiol SAMs on Cu.[29,30] They studied the air oxidation of Cu modified with SAMs of different chain lengths and found that the rates of oxidation of the Cu and the thiolates can be decreased approximately 50% by increasing the length of the SAM by four methylene units.[31] Moffat et al. found that the potential for global surface roughening of a Cu_3Au alloy was increased by adsorbing an *n*-alkanethiol SAM to the alloy.[28] Feng et al. studied the protection ability of a 1-dodecanethiol SAM on Cu surfaces that were pretreated in different ways.[32] They discovered that the passivation properties were enhanced by a nitric acid etch of the Cu prior to SAM adsorption. A series of papers by Aramaki et al. examined the corrosion resistance of Cu coated with an 11-mercapto-1-undecanol SAM linked to a second polymeric alkyltrichlorosilane layer.[33-36] They used electrochemical and spectroscopic techniques to determine the protection efficiencies of the different films and found that the polymerized SAMs are more effective at preventing corrosion than long linear-chain SAMs such as octadecanethiol.

Recently, Jennings and Laibinis discovered that SAMs prepared on UPD layers of Cu and Ag on Au are highly organized and, in the case of Ag UPD on Au, are more stable than SAMs formed on the parent metal.[3,4] This was demonstrated by measuring the extent of SAM desorption in aggressive, heated solvents and by adsorbate-exchange experiments. Burgess and Hawkridge also studied the self-assembly of octadecanethiol on Ag-UPD layers on Au using electrochemical quartz crystal microbalance (ECQCM)-based gravimetry.[37] They found that the rate of self-assembly was irreproducible on naked Au compared to the rate measured on an Ag-UPD overlayer. Although there have been several spectroscopic and electrochemical studies, to our knowledge this is the first in-situ study of Cu corrosion passivation by organomercaptan SAMs using electrochemical scanning probe techniques.

The goal of this study was to quantify the enhanced stability that different SAMs afford the Cu−UPD layer on Au and to determine the morphology of naked and thiol-modified Cu during the initial stages of corrosion. The Au/Cu−UPD electrodes were modified with monolayers of the following: $CH_3(CH_2)_4SH$, C5SH; $CH_3(CH_2)_7SH$, C8SH; $CH_3(CH_2)_{11}SH$, C12SH; $CH_3(CH_2)_{15}SH$, C16SH; $CH_3C_6H_4SH$, TC; HOC_6H_4SH, 4-HTP. The presence of the SAMs and Cu−UPD layers was verified using FTIR−external reflectance spectroscopy (FTIR-ERS) and X-ray photoelectron spectroscopy (XPS), respectively. Electrochemical and ECSTM results indicate that the potential of the UPD oxidation process and the morphology of the Cu while undergoing electro-oxidation are strongly dependent upon the type of SAM used.

Experimental Section

Chemicals. $CH_3(CH_2)_4SH$ (Aldrich, 98%), $CH_3(CH_2)_7SH$ (Aldrich, 97%), $HClO_4$ (Seastar, ultrapure), $Cu(ClO_4)_2$ (Aldrich, 98%), and 100% ethanol (Quantum Chemical Corp.) were used as received. *p*-Thiocresol, $CH_3C_6H_4SH$ (Aldrich, 98%), and 4-hydroxythiophenol, HOC_6H_4SH (Aldrich, 90%), were vacuum-sublimed. $CH_3(CH_2)_{11}SH$ (Aldrich, 98%) and $CH_3(CH_2)_{15}SH$ (Aldrich, 92%) were distilled at reduced pressure. All aqueous solutions were prepared with deionized water (Millipore, Milli-Q purification system, resistance $\approx$ 18 MΩ·cm).

Substrate Preparation. Au-coated substrates for FTIR-ERS, XPS, and voltammetry were prepared by electron-beam deposition of 100 Å of Ti followed by 2000 Å of Au onto Si(100) wafers (Lance Goddard Assoc., Foster City, CA). The Au-coated Si wafers were cleaned in a low-energy Ar plasma cleaner at medium power for 1 min (Harrick Scientific Corp., New York, Model PDC-32G) immediately prior to use. ECSTM substrates were freshly prepared single-crystal Au(111) facets on Au beads, the preparation of which has been described previously.[38-43] Briefly, melting an Au wire (0.5-mm diameter, 99.99% purity, Refining Systems Inc., Las Vegas, NV) in a H_2/O_2 flame forms a 1.5−2.0-mm-diameter ball at the end of the wire. The ball has elliptical Au(111) facets (long axis ~ 300 μm) on its surface that contain atomically flat terraces up to 1-μm wide.

SAMs were formed on Cu−UPD layers as follows: After the Au wafers or Au beads were cleaned, the substrates were immersed into a solution containing 0.01 M $Cu(ClO_4)_2$ and 0.1 M $HClO_4$ under potential control at 500 mV. The substrates were then cycled between 100 and 1500 mV at 20 mV/s until the Cu−UPD and the Au oxidation waves became well-defined (See Figure 1). The anodic peaks in Figure 1 appearing at 1100 and 1230 mV correspond to Au oxidation, while the cathodic peak at 890 mV is due to Au oxide reduction. The sharp surface waves centered at 315 mV are due to the oxidation and reduction of Cu−UPD. The scan was stopped at 50 mV (which is just prior to the onset of bulk Cu deposition as judged by STM and voltammetric measurements), and the substrate was emersed while rinsing with water. Finally, the Au/Cu−UPD substrates were rinsed with ethanol and quickly placed in the appropriate ethanolic organomercaptan solution (1−2 mM) and soaked for more than 24 h, except as noted. Upon removal from the thiol solution, the substrates were rinsed with ethanol and dried under a stream of nitrogen.

Electrochemical Measurements. All electrochemical measurements were performed using a Pine Instruments model

(19) Cooper, R. S.; Bartlett, J. H. *J. Electrochem. Soc.* **1958**, *105*, 109−116.
(20) Zhang, X. G.; Stimming, U. *Corros. Sci.* **1990**, *30*, 951−954.
(21) Morales, J.; Esparza, P.; Gonzalez, S. *Langmuir* **1996**, *12*, 500−507.
(22) Suggs, D. W.; Bard, A. J. *J. Am. Chem. Soc.* **1994**, *116*, 10725−10733.
(23) Suggs, D. W.; Bard, A. J. *J. Phys. Chem.* **1995**, *99*, 8349−8355.
(24) Kowal, K.; DeLuccia, J.; Josefowicz, J. Y.; Laird, C.; Farrington, G. C. *J. Electrochem. Soc.* **1996**, *143*, 2471−2481.
(25) Chan, H. S. O.; Ho, P. K. H.; Zhou, L.; Luo, N.; Ng, S. C.; Li, S. F. Y. *Langmuir* **1996**, *12*, 2580−2586.
(26) Pickering, H. W.; Wu, Y. C.; Gregory, D. S.; Geh, S. *J. Vac. Sci. Technol. B* **1991**, *9*, 976−983.
(27) Cruickshank, B. J.; Gewirth, A. A.; Rynders, R. M.; Alkire, R. C. *J. Electrochem. Soc.* **1992**, *139*, 2829−2832.
(28) Moffat, T. P.; Fan, F.-R. F.; Bard, A. J. *J. Electrochem. Soc.* **1991**, *138*, 3224−3235.
(29) Laibinis, P. E.; Whitesides, G. M.; Allara, D. L.; Tao, Y.-T.; Parikh, A. N.; Nuzzo, R. G. *J. Am. Chem. Soc.* **1991**, *113*, 7152−7167.
(30) Laibinis, P. E.; Whitesides, G. M. *J. Am. Chem. Soc.* **1992**, *114*, 1990−1995.
(31) Laibinis, P. E.; Whitesides, G. M. *J. Am. Chem. Soc.* **1992**, *114*, 9022−9028.
(32) Feng, Y.; Teo, W.-K.; Siow, K.-S.; Gao, Z.; Tan, K.-L.; Hsieh, A.-K. *J. Electrochem. Soc.* **1997**, *144*, 55−64.
(33) Itoh, M.; Nishihara, H.; Aramaki, K. *J. Electrochem. Soc.* **1994**, *141*, 2018−2023.
(34) Itoh, M.; Nishihara, H.; Aramaki, K. *J. Electrochem. Soc.* **1995**, *142*, 3696−3704.
(35) Itoh, M.; Nishihara, H.; Aramaki, K. *J. Electrochem. Soc.* **1995**, *142*, 1839−1846.
(36) Haneda, R.; Nishihara, H.; Aramaki, K. *J. Electrochem. Soc.* **1997**, *144*, 1215−1221.
(37) Burgess, J. D.; Hawkridge, F. M. *Langmuir* **1997**, *13*, 3781−3786.
(38) Schoer, J. K.; Ross, C. B.; Crooks, R. M.; Corbitt, T. S.; Hampden-Smith, M. J. *Langmuir* **1994**, *10*, 615−618.
(39) Snyder, S. R. *J. Electrochem. Soc.* **1992**, *139*, 5C.
(40) Ross, C. B.; Sun, L.; Crooks, R. M. *Langmuir* **1993**, *9*, 632−636.
(41) Chailapakul, O.; Crooks, R. M. *Langmuir* **1993**, *9*, 884−888.
(42) Hsu, T.; Cowley, J. M. *Ultramicroscopy* **1983**, *11*, 239−250.
(43) Sun, L.; Crooks, R. M. *J. Electrochem. Soc.* **1991**, *138*, L23−L25.

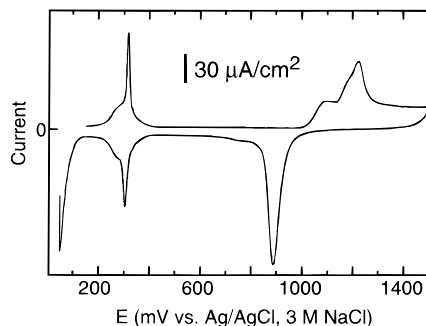

Figure 1. Cyclic voltammogram of Au obtained in 0.01 M $Cu(ClO_4)_2$ and 0.1 M $HClO_4$ showing a clean Au surface with well-defined Au oxidation, Au oxide reduction, and Cu–UPD peaks. The Au/Cu–UPD/SAM composite electrodes were prepared by removing the Au substrate at a potential where a Cu–UPD layer remains on the surface (50 mV) and then adsorbing the SAM from an ethanolic solution.

AFCBP1 bipotentiostat (Grove City, PA). The data were recorded on a Kipp and Zonen X–Y recorder. The cell, fabricated from Kel-F, was designed to expose a 0.25-cm^2 working area of the Au wafer to the electrolyte solution. The approximately 15-mL cell volume accommodates a Pt counter electrode and an Ag/AgCl, 3 M NaCl, reference electrode (BAS, West Lafayette, IN), against which all potentials are reported. The substrates were immersed in air-saturated 0.1 M $HClO_4$ electrolyte solutions at −200 mV. For linear sweep voltammetry (LSV), the voltage was scanned at 10 mV/s and the first anodic scan was recorded to 1700 mV for the different electrodes. For cyclic voltammetry (CV), the voltage was cycled between −200 and 1500 mV, stopping at −200 mV between successive scans.

FTIR-ERS Measurements. FTIR-ERS measurements were made using a Bio-Rad Digilab FTS-40 spectrometer equipped with a Harrick Scientific Seagull reflection accessory and a liquid-N_2-cooled MCT detector.[44] All spectra were obtained using *p*-polarized light at an 84° angle of incidence with respect to the substrate normal. Spectra are the sum of 256 or fewer individual scans. None of the spectra were baseline-corrected except Figure 5B, which was baseline-corrected using six points. The reference spectra were obtained on unmodified Au substrates.

XPS Measurements. XPS measurements were made using a Perkin-Elmer PHI 5500 spectrometer having a Mg anode at 400 W and pressures less than 7×10^{-8} mmHg. The pass energy was 29.35 eV with a 0.125-eV step size. Survey scans were acquired between 1100 and 0 eV, and high-resolution scans were acquired for Cu. Photoelectrons were detected at a 45° takeoff angle. Each sample was exposed to the X-ray source for less than 1 h. All XPS peak positions were referenced to the Au ($4f_{7/2}$) peak at 84.0 eV.[3]

ECSTM Measurements. A Nanoscope III ECSTM (Digital Instruments, Santa Barbara, CA) equipped with an integral bipotentiostat was used for data acquisition. The tips were mechanically cut 80/20 Pt/Ir (Digital Instruments, Santa Barbara, CA) and coated with Apiezon wax to minimize Faradaic current, which was typically 10–20 pA (measured by cycling the tip between +0.1 V and −0.1 V vs a Pt wire in 0.1 M KCl). The 25-mL Kel-F ECSTM cell[2] is large enough to accommodate a true reference electrode (Ag/AgCl, 3 M NaCl, BAS, West Lafayette, IN), against which all potentials are reported. A Pt wire counter electrode completed the cell.

All ECSTM images were obtained in the constant-current mode. The tip was biased 50 mV positive of the substrate. Scan rates of 3–5 Hz, which correspond to about one image per minute, were used. All substrates were immersed at −200 mV unless otherwise noted. For the Cu–UPD-stripping experiments, consecutive images were obtained at 25-mV potential increments, except during Cu–UPD oxidation, where increments of 10 mV were used. Images of regions larger than those presented in the figures were regularly acquired during each experiment to check for evidence of tip effects. The *z*-scale was 2 nm in all images, and the tunneling current was varied between 200 pA and 1.0 nA. The potentials at which the images were acquired are noted in the figures.

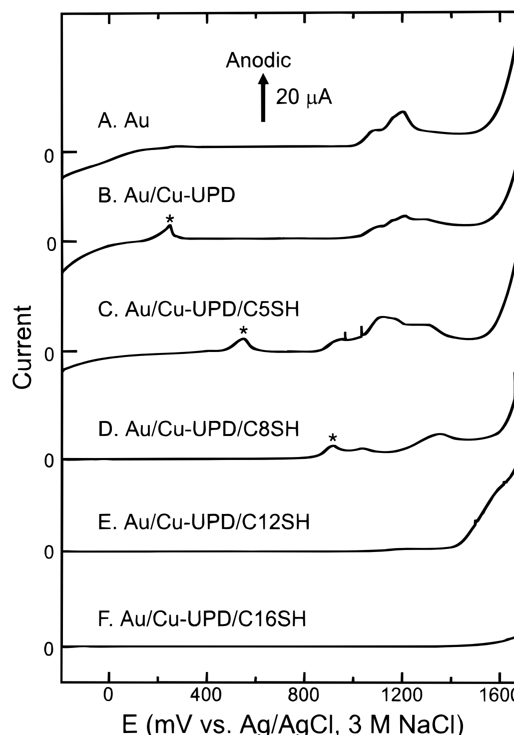

Figure 2. Linear sweep voltammograms of (A) Au, (B) Au/Cu–UPD, (C) Au/Cu–UPD/C5SH, (D) Au/Cu–UPD/C8SH, (E) Au/Cu–UPD/C12SH, and (F) Au/Cu–UPD/C16SH introduced into 0.1 M $HClO_4$ at −200 mV and scanned positive to 1700 mV at 10 mV/s. The anodic peaks noted by the asterisks in parts B–D result from oxidation of the Cu–UPD monolayer. These data show that the oxidation potential of the Cu–UPD increases with increasing SAM thickness. For the longer chain SAMs, as in parts E and F, neither Cu nor Au oxidation is observed.

Results and Discussion

Voltammetric Characterization. Figure 2 shows linear sweep voltammograms (LSVs) obtained in 0.1 M $HClO_4$ of naked Au, Au/Cu–UPD, and a series of *n*-alkanethiol SAM-coated electrodes (Au/Cu–UPD/CnSH). For the naked Au electrode (Figure 2A), no anodic waves are observed at potentials less than 1000 mV. The peaks at 1100 and 1200 mV correspond to Au oxidation, and the rising anodic current apparent at potentials greater than 1500 mV is due to solvent electrolysis. The cathodic background current observed at negative potentials is due to the reduction of O_2. The response of an Au/Cu–UPD electrode is shown in Figure 2B, where the Cu–UPD stripping wave (noted by the asterisk) is centered at 235 mV. This peak is 80 mV negative of the Cu–UPD peak observed in Figure 1, which is a thermodynamic consequence of having no Cu^{2+} in the electrolyte solution. The Au oxidation peaks are also present at potentials above 1000 mV.

Figure 2C–F shows the results obtained for the SAM-modified Au/Cu–UPD surfaces. The Cu stripping wave for Au/Cu–UPD/C5SH is shifted to 550 mV (Figure 2C), which is 315 mV positive of that observed for Au/Cu–UPD. There is another anodic peak at 950 mV, which was not observed in the LSV of the naked Au or Au/Cu–UPD. This might arise from oxidation of the thiol

(44) Crooks, R. M.; Sun, L.; Xu, C.; Hill, S. L.; Ricco, A. J. *Spectroscopy* **1993**, *8*, 28.

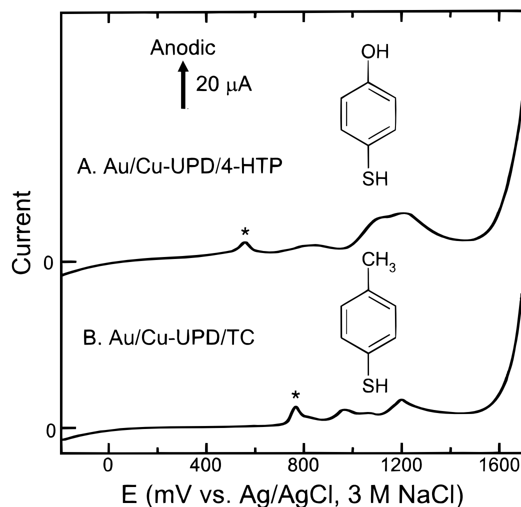

Figure 3. Linear sweep voltammograms of (A) Au/Cu−UPD/4-HTP and (B) Au/Cu−UPD/TC introduced into 0.1 M $HClO_4$ at −200 mV and scanned positive to 1700 mV at 10 mV/s. The anodic peaks noted by the asterisks result from oxidation of the Cu−UPD monolayer. These data show that, for aromatic SAMs, the CH_3 end group provides better protection than the OH end group. Also, comparing the LSV of Au/Cu−UPD/TC to that of Au/Cu−UPD/C5SH (Figure 2C) leads to the conclusion that aromatic SAMs protect better than linear-chain SAMs, since both of the monolayers are of approximately equal thickness and contain a CH_3 end group.

functional groups of the C5SH SAM.[45] The Au oxidation waves are poorly defined on all of the SAM-modified surfaces. The Cu stripping wave for Au/Cu−UPD/C8SH is present at 910 mV (Figure 2D), which represents a shift of 675 mV relative to that for Au/Cu−UPD. There is a smaller peak at 1030 mV, which is due either to Cu oxidation from different surface sites or to C8SH oxidation. The Au/Cu−UPD/C12SH electrode (Figure 2E) prevents Cu stripping up to potentials of at least 1100 mV, but there is a slight anodic current around 1200 mV that increases significantly above 1400 mV. At these extreme positive potentials the voltammetry becomes complicated and difficult to interpret because several Faradaic processes could be occurring simultaneously. Among these are Cu stripping, Au oxidation, oxidation of the SAM, and solvent oxidation. The C16SH monolayer (Figure 2F) completely prevents the electro-oxidation of Cu up to at least 1500 mV. The current observed at the most extreme positive potentials probably corresponds to oxygen evolution, but XPS data discussed later confirm that the Cu−UPD layer remains on the surface. Also note the absence of a voltammetric signature for Au oxidation (see Figure 2A).

There are three observable trends in the LSVs of Figure 2: as the thickness of the SAM increases, the cathodic current due to reduction of oxygen at −200 mV decreases, the anodic stripping wave for Cu shifts positive, and the anodic peak due to Au oxidation shifts positive. The passivation of the Au/Cu−UPD/C16SH surface is particularly remarkable and will be discussed in more detail later.

Figure 3 shows the LSVs of two Au/Cu−UPD surfaces modified with SAMs composed of aromatic thiols having a hydrophilic and a hydrophobic end group. The OH-terminated Au/Cu−UPD/4-HTP surface exhibits a Cu−UPD stripping wave at 560 mV (Figure 3A) at a potential similar to that for the Au/Cu−UPD/C5SH surface (Figure 2C). There is also a broad peak around 900 mV, which may be due to an electrochemical reaction involving the SAM,[46] and peaks corresponding to Au oxidation at potentials above 1000 mV. The Cu stripping wave from the CH_3-terminated Au/Cu−UPD/TC surface appears at 780 mV (Figure 3B), indicating superior corrosion passivation compared to that for Au/Cu−UPD/4-HTP. The data in Figure 3 also show that aromatic SAMs are more effective passivation layers than linear-chain SAMs of equal thickness, since both the 4-HTP and the TC protect the Cu−UPD layer better than the equally thick C5SH SAM (Figure 2C).

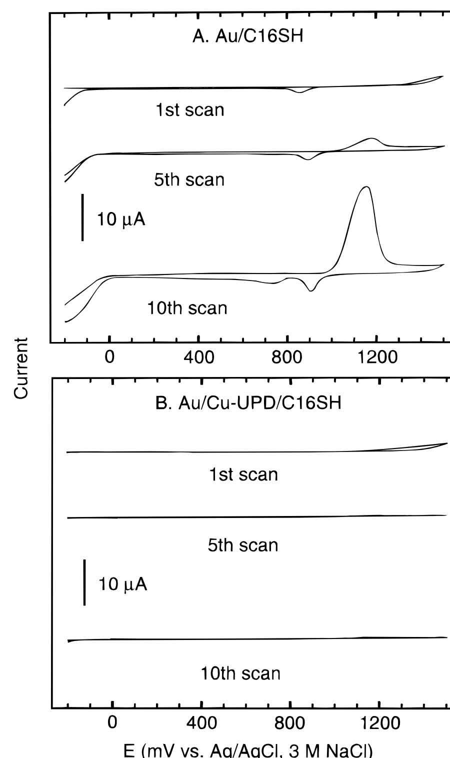

Figure 4. Cyclic voltammograms obtained in 0.1 M $HClO_4$ of the first, fifth, and tenth scans between −200 and 1500 mV at 10 mV/s of (A) Au/C16SH and (B) Au/Cu−UPD/C16SH. The electrodes were soaked in the organomercaptan for 2−3 h prior to data acquisition. This comparison shows that the Cu−UPD layer adds to the stability of the SAM and leads to greater resistance toward Au oxidation.

Figure 4 demonstrates that the passivating ability of C16SH immobilized on Au/Cu−UPD is far superior to that observed for C16SH adsorbed to naked Au. Figure 4A shows the cyclic voltammetry of the first, fifth, and tenth scans of Au/C16SH in 0.1 M $HClO_4$. On the first scan there is very little current due to Au oxidation, indicating that C16SH initially passivates the surface. By the tenth scan, however, the current increases significantly as the SAM becomes disordered and desorbs from the surface. Figure 4B contrasts this behavior with that observed for Au/Cu−UPD/C16SH, which protects the Au from surface oxidation remarkably well for at least the first 10 scans. The results clearly indicate that the barrier properties of the SAM, and thus the corrosion passivation properties, improve markedly in the presence of the Cu−UPD adhesion layer. A possible explanation for this behavior is that the Cu−UPD/SAM interaction is stronger than the Au/SAM interaction. Alternatively, the Cu−UPD layer might serve as a better template surface for thiol

(45) Widrig, C. A.; Chung, C.; Porter, M. D. *J. Electroanal. Chem.* **1991**, *310*, 335−359.

(46) This broad wave could be due to oxidation of the thiolate; however, phenols are also known to polymerize at positive potentials.

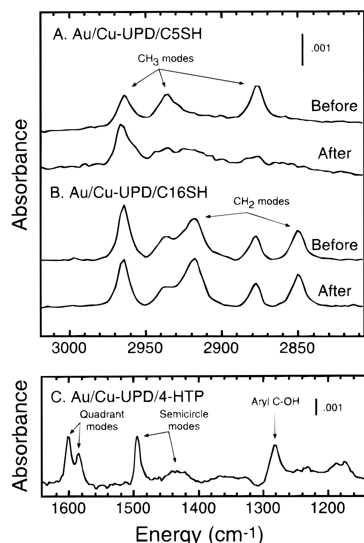

Figure 5. FTIR-ERS spectra of (A) Au/Cu−UPD/C5SH, (B) Au/Cu−UPD/C16SH, and (C) Au/Cu−UPD/4-HTP. The bottom spectra in parts A and B are after scanning at 10 mV/s from −200 to 900 and 1500 mV, respectively, in 0.1 M $HClO_4$ electrolyte. The C5SH spectrum shows significant loss of the CH_3 symmetric modes, while the C16SH spectrum remains unchanged after the scan to 1500 mV. The spectrum of Au/Cu−UPD/4-HTP after scanning positive to 1000 mV is not shown because no peaks attributable to 4-HTP were observed.

self-assembly than Au, which leads to better packing of the monolayer and fewer defects.

FTIR-ERS Characterization. The FTIR-ERS spectra in Figure 5 confirm that SAMs form on Au/Cu−UPD[3] and that the longer C16SH SAM is more stable than the shorter C5SH and 4-HTP SAMs after scanning to positive potentials. The top spectrum in Figure 5A shows the hydrocarbon stretching region for an Au/Cu−UPD/C5SH surface. The peak positions and relative sizes are comparable to those for previously reported spectra of C3SH, C5SH, and C7SH on Au.[47−49] The peaks at 2964, 2936, and 2877 cm^{-1} arise from CH_3 modes. The absence of distinct bands attributable to asymmetric and symmetric CH_2 stretching modes between 2919 and 2925 cm^{-1} and between 2850 and 2855 cm^{-1}, respectively, may indicate that the monolayer is disordered and of lower coverage than is observed for the long-chain *n*-alkanethiols (Figure 5B).[47] Alternatively, the orientation of the methylene C−H dipoles may render them IR silent.[50] After a potential scan from −200 to 900 mV in 0.1 M $HClO_4$ (bottom spectrum, Figure 5A), the symmetric CH_3 modes mostly disappear while the asymmetric CH_3 mode actually increases. This is consistent with the monolayer being highly disordered, of lower coverage, and in a conformation where the alkane chain is near parallel to the surface plane.[50] This is anticipated, since the underlying Cu−UPD has been oxidatively stripped.

The top spectrum in Figure 5B shows the hydrocarbon region for an Au/Cu−UPD/C16SH surface. The CH_3 modes are observed in the same locations as for the C5SH monolayer before Cu oxidation, but they are accompanied by asymmetric and symmetric CH_2 stretches at 2919 and 2850 cm^{-1}, respectively, consistent with literature reports for highly ordered C16SH SAMs on Au.[47] This result is in contradistinction to previous reports for $CH_3(CH_2)_{17}$-SH on Au/Cu−UPD, where the asymmetric and symmetric CH_2 stretches were found to be shifted toward higher energy by 2−3 cm^{-1}, indicating a lower degree of order.[3] This discrepancy can be attributed to different soaking times (40 min compared to 24 h in the present study) and possibly to the use of a different supporting electrolyte for Cu deposition: compared to H_2SO_4, $HClO_4$ has been found to lead to more close-packed Cu.[7] Consistent with Jennings and Laibinis,[3] we find that the intensity of the asymmetric CH_2 stretch is lower for the C16SH monolayer on Au/Cu−UPD compared to that observed on naked Au. They speculated that the decrease in intensity is due to less tilting of the alkane chain.[50] The bottom spectrum is the same surface after scanning from −200 to 1500 mV in 0.1 M $HClO_4$. In contrast to the case for the Au/Cu−UPD/C5SH surface, there is little or no difference between the hydrocarbon regions in the top and bottom spectra. The CH_2 and CH_3 modes are located in the same position and are of nearly equal intensity. Together with the previously discussed electrochemical data and the XPS data that follow, these results indicate that the SAM monolayer remains intact and highly ordered even after scanning the potential to 1500 mV.

Figure 5C shows an IR spectrum of Au/Cu−UPD/4-HTP. The spectrum is similar to that for 4-HTP on Au,[51] except that all of the peaks are shifted to higher energy. For example, we observe the two aryl quadrant stretch modes at 1601 and 1585 cm^{-1} in the Au/Cu−UPD/4-HTP spectrum, which occur at 1594 and 1579 cm^{-1}, respectively, for Au/4-HTP. The C−OH stretch for Au/Cu−UPD/4-HTP is located at 1283 cm^{-1} but shifted down in energy by 19 cm^{-1} for Au/4-HTP. We believe that these shifts are due to the Cu being more electropositive than Au,[52] resulting in the thiol carrying more electron density when adsorbed on Au/Cu−UPD than when adsorbed on naked Au. This additional electron density is distributed over the entire molecule with the majority residing in the aryl−OH bond, hence the 19 cm^{-1} shift in the C−OH stretch. These subtle shifts in the vibrational spectra, which are not apparent for the unconjugated alkanethiols, may provide guidance as to the means by which SAMs on UPD metals are rendered more stable than those on naked Au. No peaks were observed in the IR spectrum after scanning the Au/Cu−UPD/4-HTP surface from −200 to 1000 mV in 0.1 M $HClO_4$.

The results obtained for the surfaces after scanning to positive potentials, where Au/Cu−UPD oxidizes, are consistent with the electrochemical data and the XPS data described in the next section. FTIR-ERS spectra were also obtained for the other SAMs whose linear sweep voltammograms are shown in Figures 2 and 3. The spectra (data not shown) confirmed that these SAMs also form on Cu−UPD and were comparable with spectra reported for the same SAMs on naked Au.

XPS Characterization. Figure 6 shows XPS data obtained for naked and SAM-coated Au/Cu−UPD surfaces prepared identically to those used to obtain the data shown in Figure 5. The spectrum of naked Au/Cu−UPD and the top spectra shown for the three pairs of SAM-modified electrodes reveal the $Cu(2p_{3/2})$ and $Cu(2p_{1/2})$ peaks located at 931.1 and 950.8 eV, respectively, indicating the presence of either Cu(0) or Cu(I). Unfortunately, XPS cannot

(47) Porter, M. D.; Bright, T. B.; Allara, D. L.; Chidsey, C. E. D. *J. Am. Chem. Soc.* **1987**, *109*, 3559−3568.
(48) Sun, L.; Kepley, L. J.; Crooks, R. M. *Langmuir* **1992**, *8*, 2101−2103.
(49) Chailapakul, O.; Sun, L.; Xu, C.; Crooks, R. M. *J. Am. Chem. Soc.* **1993**, *115*, 12459−12467.
(50) Porter, M. D. *Anal. Chem.* **1988**, *60*, 1143A−1155A.
(51) Xu, C.; Sun, L.; Kepley, L. J.; Crooks, R. M.; Ricco, A. J. *Anal. Chem.* **1993**, *65*, 2102−2107.
(52) *CRC Handbook of Chemistry and Physics*, 71st ed.; Lide, D. R., Ed.; CRC Press: Boston, 1990.

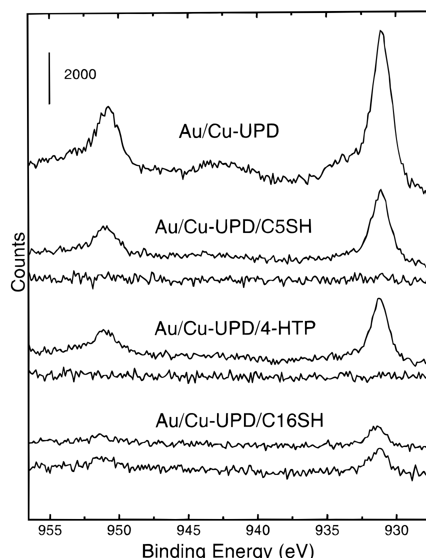

Figure 6. XPS spectra of Au/Cu−UPD and Au/Cu−UPD/SAM electrodes in the Cu(2p) region (top) before scanning to Cu−UPD oxidation potentials and (bottom) after scanning past the Au/Cu−UPD oxidation potential. Each pair of spectra was obtained on two different substrates that were treated identically, except that the substrates used to obtain the bottom spectra of each pair were immersed into $HClO_4$ at −200 mV and scanned to 900, 1000, and 1500 mV on the Au/Cu−UPD/C5SH, Au/Cu−UPD/4-HTP, and Au/Cu−UPD/C16SH surfaces, respectively. It is apparent from the spectra obtained prior to scanning that the Cu−UPD survives the self-assembly process. After stripping, Cu is absent in the C5SH and 4-HTP spectra, but the C16SH surface shows little or no Cu loss.

distinguish between these two possibilities,[53] but the four-peak pattern characteristic of Cu(II) is definitely not observed.[54] The Cu XPS signal decreases as the monolayer thickness increases, which is consistent with the findings of Bain and Whitesides for SAMs on Au.[55] The lower spectra were obtained after immersing identically prepared electrodes into aqueous $HClO_4$ at −200 mV and scanning to 900, 1000, and 1500 mV for the C5SH-, 4-HTP-, and C16SH-modified Au/Cu−UPD surfaces, respectively. The pairs of spectra shown for the C5SH and 4-HTP SAMs indicate that all of the Cu desorbs during the scan, while there is little or no loss of Cu from the Au/Cu−UPD/C16SH surface. This is consistent with the spectroscopic and electrochemical data, which support Cu−UPD stripping on the C5SH and 4-HTP surfaces but not on the C16SH. These data also support our contention that the first anodic peak observed in all of the linear sweep voltammograms in Figures 2 and 3 (except Figure 2A, E, and F) is due to Cu−UPD oxidation.

ECSTM Results. Figure 7 shows 300 nm × 300 nm ECSTM images of Au, Au/Cu−UPD, and SAM-modified Au/Cu−UPD electrodes obtained in aqueous 0.1 M $HClO_4$. At least one Au(111) atomic step edge (0.235 nm in height)[10,56] is included in each image as an internal reference for the *z*-scale normal to the surface. Figure 7A shows an unmodified Au(111) electrode at 200 mV. The surface reveals Au monatomic steps, and its topographical features are stable up to ∼600 mV, where Cl^- impurities (present in the $HClO_4$ electrolyte) adsorb strongly, enhance the mobility of surface Au atoms, and reduce the extent of surface roughness.[57] At 800 mV (Figure 7B), Cl^- begins to dissolve the Au preferentially at step edges and other high-energy defect sites, while the terraces remain unchanged. At 1000 mV (Figure 7C), which is near the foot of the Au oxidation wave, the potential is sufficiently positive to cause pitting on the terraces in addition to corrosion along the step edges. An oxide layer also forms slowly on the Au, which leads to passivation of the surface at more positive potentials. These data are significant because they show that, in $HClO_4$, the Au surface does not change until potentials above 600 mV. In the following ECSTM images, we monitored the stripping of Cu−UPD layers in the potential range −200 to 350 mV for Au/Cu−UPD, Au/Cu−UPD/C5SH, and Au/Cu−UPD/4-HTP surfaces. The control experiment represented by parts A−C of Figure 7 indicates that any morphology changes arise from the Cu−UPD layer not the underlying Au.

Parts D−F of Figure 7 show the ECSTM images of an Au/Cu−UPD electrode over a potential range where Cu is electro-oxidized. Figure 7D shows the surface at −50 mV, which is almost fully covered with Cu−UPD. For a given terrace, Cu is represented by the lighter-colored domains uniformly distributed over the surface, while the darker regions correspond to exposed areas of the underlying Au. The white, circular islands in the image most likely correspond to a different phase of Cu than the lighter-colored Cu domains. The appearance of such islands has been previously observed in a Cu−UPD study on Au(111) and attributed to a stable Cu (1 × 1) phase, which was found to extend higher above the Au surface than the other two phases observed for Cu−UPD on Au-(111).[10] Figure 7E shows the same electrode at 150 mV where some Cu has oxidized, leaving approximately half coverage of the Cu−UPD layer. The Cu−UPD layer oxidizes homogeneously with no apparent topological preference for step edges or other specific sites, which is distinctly different from dissolution of bulk Cu(111) in Cl^-.[22] Figure 7F shows the same electrode at 200 mV after most of the Cu monolayer has dissolved. More Cu (1 × 1) islands form as the last of the lighter Cu−UPD regions corrode. These Cu (1 × 1) islands do not disappear until potentials exceeding 300 mV, because they are more stable than the rest of the Cu−UPD layer. It is worth noting that the half-coverage potential according to our ECSTM data is approximately 85 mV negative of the Cu−UPD oxidation peak observed in the voltammetry (Figure 2B). We attribute this discrepancy to the many differences in the ECSTM and LSV experiments, such as scan rates, cell geometries, and substrates. This discrepancy exists in all of the ECSTM data. The important point, however, is that the relative trends in the ECSTM data are in excellent agreement with the voltammetric, XPS, and FTIR results.

Parts G−I of Figure 7 show ECSTM images of an Au/Cu−UPD/C5SH electrode. Figure 7G was acquired at −75 mV with nearly a full Cu−UPD layer present. The dark pits are areas of exposed Au where part of the Cu−UPD layer is missing. The image in Figure 7H shows an intermediate Cu coverage at 210 mV. The corrosion process proceeds uniformly, yielding a weblike structure of the remaining Cu, represented by the bright areas distributed over the surface. The weblike strands are of nearly equal width and thickness, and line scans across them reveal that the Cu−Au step height is 0.10−0.12 nm,

(53) *Practical Surface Analysis*, 2nd ed.; Briggs, D., Seah, M. P., Eds.; John Wiley & Sons: New York, 1990; Vol. 1, pp 487−529.
(54) Wagner, C. D.; Kiggs, W. M.; Davis, L. E.; Moulder, J. F. *Handbook of X-ray Photoelectron Spectroscopy*; Perkin-Elmer Corporation-Physical Electronics Division: Eden Prairie, MN, 1979.
(55) Bain, C. D.; Whitesides, G. M. *J. Phys. Chem.* **1989**, *93*, 1670−1673.
(56) Honbo, H.; Sugawara, S.; Itaya, K. *Anal. Chem.* **1990**, *62*, 2424−2429.
(57) Trevor, D. J.; Chidsey, C. E. D.; Loiacono, D. N. *Phys. Rev. Lett.* **1989**, *62*, 929−932.

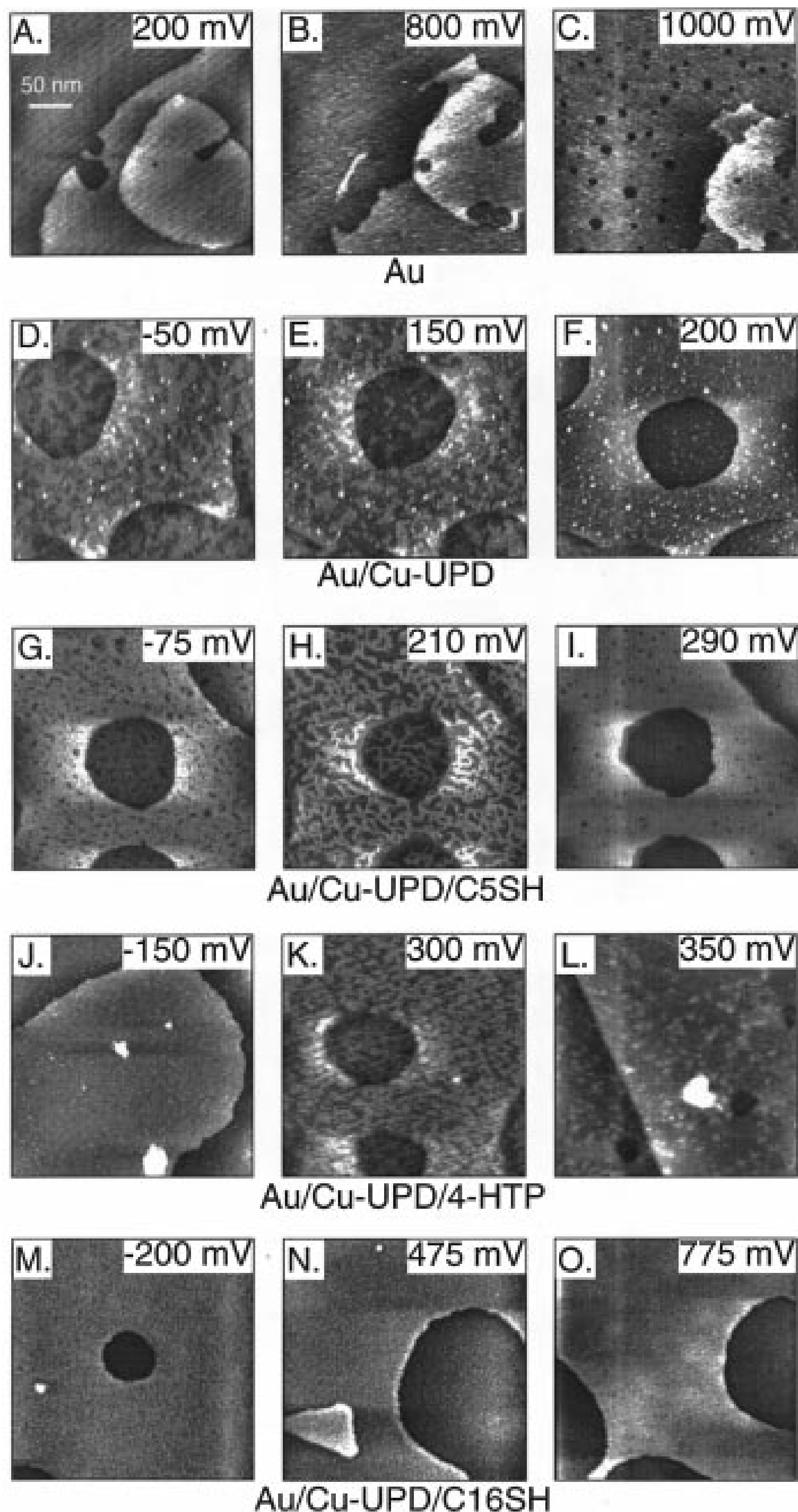

Figure 7. 300 nm × 300 nm ECSTM images obtained in 0.1 M $HClO_4$ of (A−C) Au, (D−F) Au/Cu−UPD, (G−I) Au/Cu−UPD/C5SH, (J−L) Au/Cu−UPD/4-HTP, and (M−O) Au/Cu−UPD/C16SH. The Au surface in parts A−C was introduced into the electrolyte at +200 mV, while the naked and SAM-modified Cu−UPD surfaces were introduced at −200 mV. The bias voltage was 50 mV, and the tunneling current ranged between 200 pA and 1.0 nA. The *z*-range in all of the images is 2 nm. Images (J−O) were not obtained in the same region because of tip-induced damage to the surface.

which is less than the Au−Au step height of approximately 0.24 nm. The Cu−Au step height is consistent with a Cu (5 × 5) adlattice structure,[10] provided that the C5SH monolayer does not significantly affect the tunneling distance between the tip and the surface. Note that, on the naked surface (Figure 7F), nearly all of the Cu is dissolved at 200 mV, but the remainder of the Cu on the C5SH-coated surface does not fully strip until 290 mV (Figure 7I), leaving behind a surface decorated with a low density of monatomic pits in the Au.

Parts J−L of Figure 7 show ECSTM data for an Au/Cu−UPD/4-HTP composite electrode. At −150 mV (Figure 7J), a complete Cu monolayer is stable on the Au surface. Figure 7K shows the same electrode having an intermediate Cu coverage at 300 mV. The corrosion of the Au/Cu−UPD/4-HTP occurs homogeneously over the entire surface with no apparent preference for one region over another. The surface is distinctly different from the C5SH-modified surface at nearly equal Cu coverage (Figure 7H). The Cu remains in domains of various sizes rather than weblike strands of equal width and height. Although the Cu coverage is similar to that of the C5SH-modified surface, the potential is 90 mV more positive, revealing that 4-HTP passivates the Cu more effectively (even though the monolayers are of approximately equal thickness). This trend is consistent with the voltammetry. Figure 7L shows the surface at 350 mV after most of the Cu is electro-oxidized. The potential is 60 mV more positive than that of the C5SH surface (Figure 7I), yet some small Cu islands still remain on the 4-HTP-modified surface. The potential is 150 mV more positive than that of the naked Cu−UPD surface (Figure 7F), which had almost no Cu remaining at 200 mV.

Parts M−O of Figure 7 show the images of an Au/Cu−UPD/C16SH composite electrode. Figure 7M was obtained at −200 mV, where there is a full Cu monolayer. It is interesting to note that the surface does not contain any of the monatomic "thiol-induced pits" routinely observed in STM studies of long, linear-chain *n*-alkanethiol monolayers on Au(111).[40,58−60] At 475 mV (Figure 7N) there is no indication of any Cu−UPD stripping, and even at 775 mV (Figure 7O) the Cu layer remains unchanged. At potentials as high as 1500 mV, the STM data indicate no further changes to the surface or evidence of Cu oxidation (data not shown). In addition to preventing the oxidation of Cu (at least 1200 mV past its oxidation potential on naked Au(111)/Cu−UPD), this film also prevents dissolution of the Au by Cl^- and Au oxidation.

(58) Sun, L.; Crooks, R. M. *Langmuir* **1993**, *9*, 1951.
(59) Kim, Y.-T.; Bard, A. J. *Langmuir* **1992**, *8*, 1096.
(60) Edinger, K.; Golzhauser, A.; Demota, K.; Woll, C.; Grunze, M. *Langmuir* **1993**, *9*, 4−8.

Summary and Conclusions

Previously, we demonstrated that organomercaptan SAMs retard the corrosion of metal surfaces.[1,2] However, we concluded that SAMs were insufficiently stable to be of much technological significance. Following the discovery by Jennings and Laibinis that UPD layers of coinage metals enhance SAM stability, we are more optimistic now about the technological significance of these composite materials as ultrathin corrosion passivation layers. All of the monolayers, when formed on top of a Cu−UPD layer, shift the electro-oxidation of Cu to more positive potentials relative to that of the untreated Cu−UPD layer. The morphology of the Cu during corrosion and the extent to which the Cu−UPD is passivated strongly depend upon the type of thiol adsorbed. The SAMs in this study enhance metal passivation in the following order: C16SH > C12SH > C8SH > TC > 4-HTP > C5SH.

The amount of corrosion protection afforded to the UPD layer of Cu with extremely thin monolayers such as TC, 4-HTP, and C5SH (<1.0 nm thick) is remarkable. Since the TC protects better than the 4-HTP, we conclude that CH_3-terminated aromatic SAMs are superior to OH-terminated aromatic SAMs. Since TC protects Cu−UPD better than C5SH and the two monolayers are approximately equal in thickness and contain the same CH_3 end group, we conclude that aromatic SAMs offer superior protection compared to linear-chain SAMs. Shifts in the IR peak positions suggest this may be a consequence of a stronger bond between the aromatic thiols and Cu compared to that for the *n*-alkanethiols. The amount of protection gained by the longer C16SH (<3.0 nm thick) on Cu−UPD is astonishing. Not only does the C16SH effectively passivate the Cu−UPD, but the combination of the C16SH and the Cu−UPD layer enhances the nobility of the underlying Au to a greater extent than the C16SH SAM alone. This strategy has real possibilities for increasing the corrosion resistance of protective coatings on more practical and commercially important metals.

Acknowledgment. We gratefully acknowledge the Office of Naval Research for full support of this work.

LA970905Z